

STIMULUS: Noninvasive Dynamic Patterns of Neurostimulation Using Spatio-Temporal Interference

Jiaming Cao and Pulkit Grover

Carnegie Mellon University, Pittsburgh, United States

{jiamingc, pgrover}@andrew.cmu.edu

Abstract— Objective: This paper obtains strategies that can achieve spatially precise noninvasive deep brain stimulation using electrical currents. **Methods:** We provide the *Spatio-Temporal Interference-based stiMULATION focUsing Strategy* (STIMULUS), that generates rich patterns of spatiotemporally interfering currents to stimulate precisely and deep inside the brain. To calibrate and compare the accuracy of stimulation using different techniques, we utilize computational Hodgkin-Huxley-type models for neurons and a model of current dispersion in the head. **Results:** In this computational model, STIMULUS dramatically outperforms the recently proposed Temporal Interference (TI) stimulation strategy in spatial precision. Our results also suggest that STIMULUS can attain steerable and multisite stimulation which can be important in giving feedback in brain-machine interfaces. Finally, by examining more mammalian neuron-types, we also observe that not every neuron exhibits temporal-interference stimulation. **Conclusions:** Computer simulations suggest that the proposed STIMULUS strategy has potential to achieve noninvasive electrical deep brain stimulation with high spatial precision, and further, has the flexibility of generating rich stimulation patterns. That some neuron-types do not exhibit TI stimulation suggests that caution is needed in evaluating conclusions of application of TI stimulation on mammalian brains. **Significance:** A technique to reliably, noninvasively, and precisely stimulate deep inside the human brain could revolutionize human neuroscience and clinical treatments. We obtain the first computational demonstration of the recently proposed TI stimulation. Advancing on that, we propose a novel strategy that can perform stimulation with high precision and flexibility.

I. INTRODUCTION

HIGH precision noninvasive stimulation of the brain can transform neuroscience, brain-machine interfaces, and clinical treatments of neural disorders. The problem is challenging. Laws of physics dictate that electromagnetic waves disperse with distance from the scalp, which reduces their spatial resolution for deep stimulation in particular. While ultrasound, which has less dispersion, appears to be a promising alternative, its efficacy and mechanisms are less well understood¹. Understanding mechanisms using biological models is an important validation step for any modality.

In this paper, we use biological models to obtain noninvasive multielectrode current stimulation techniques that exploit the

This work expands on our recent conference paper [1] that explored mechanisms of TI stimulation and whether single neuron models exhibit TI stimulation. We acknowledge support of NSF CNS-1702694 and CMU BrainHUB, and thank Alison Barth, Brent Doiron, Sanghamitra Dutta, Manu Gopakumar, Max Jin, Jana Kainerstorfer, Shawn Kelly, Praveen Venkatesh, Alireza Chaman Zar and Chaitanya Goswami for helpful discussions.

¹See recent experimental evidence in this direction [2], [3] that has further been challenged with experimental evidence in [4].

knowledge of the physics of dispersion, and of the biology of how a neuron reacts to an external current, to improve spatial precision and stimulate deep inside the brain. We advance on the recent work of Grossman *et al.* [5], which develops a “Temporal Interference” (TI) stimulation strategy that, in *in vivo* mice experiments, appears to engage neurons far from the electrodes without stimulating those close to the electrodes. The strategy was used earlier under the name of “Interferential Stimulation” in e.g., electroanesthesia and peripheral nerve stimulation ([6], [7], and the references therein). This approach holds promise, but, the mechanisms behind TI stimulation are not well understood, and crucially, as Grossman *et al.* themselves note, the precision and depth need to be dramatically improved for such techniques to be applicable to human brains.

In this paper, we first obtain a deeper understanding of TI stimulation by demonstrating that qualitatively, results of [5] can be recovered in a computational model where brain is modeled as a “sea of neurons”. This result, and the fact that it can be obtained in simplistic models, is significant: understanding TI stimulation through existing computational models not only serves as a much-needed validation of TI stimulation (as noted above), it also enables us to improve on the TI stimulation strategies as initially proposed. There is one caveat, however: as we discuss below (and in detail in Section III-B), only some neuron-types exhibit TI stimulation.

We consider the case in which one is interested in stimulating a small but precisely defined *target region* in the brain. Ideally, all neurons in the region should be stimulated, and stimulation outside this target region should be minimal. We show that in our model, the TI strategy can fail to stimulate the entire desired region of stimulation, and also results in engagement of shallow neurons. As an improvement, we first generalize TI stimulation to multiple (> 2) electrode-pairs, which succeeds in reducing shallow stimulation, but does not eliminate it, and is still unable to achieve high spatial precision. To actively combat these drawbacks of multielectrode TI stimulation (namely, coverage of target regions and shallow engagement), we propose “Spatio-Temporal Interference-based stiMULATION focUsing Strategies” (STIMULUS) that harness the spatial diversity of current dispersion to improve the spatial precision of stimulation.

In a recent conference paper [1], we attempted to gain an understanding of the mechanisms of 2-electrode-pair TI stimulation, and examined whether single neuron models for different neuron-types exhibit TI stimulation. For the three neuron-types considered in that work, we showed that both

the original Hodgkin-Huxley squid neuron [8] and an excitatory mammalian neuron [9] exhibit properties consistent with TI stimulation, whereas an inhibitory parvalbumin-expressing neuron [10], [11] does not. In the current work we utilize the understanding gained in [1] to develop novel stimulation strategies. In part, this addresses the open question raised in [1] on whether (for neuron-types for which it does succeed) the spatial precision of 2-electrode-pair TI stimulation can be improved and undesired shallow stimulation can be reduced by using multiple electrode pairs with carefully chosen current waveforms and amplitudes. For completeness, we also include some relevant results from [1] (in Section III-B).

We next review the fundamentals of temporal interference stimulation, examine its limitations, and describe how our strategy is capable of overcoming some of these limitations.

Review of TI stimulation: TI stimulation [5] is based on simultaneous application of two sinusoidal currents of slightly different frequencies to produce temporal interference patterns. In mice models, Grossman *et al.* observe that neurons near the surface are not stimulated despite stimulation of neurons deeper in the brain. The key intuition behind TI stimulation is as follows (see Fig. 3): it is well known that neurons do not respond to high frequency sinusoidal current stimulation [12]. However, at locations where the sinusoidal currents have comparable amplitudes, addition of two high-frequency sinusoidal currents of slightly different frequencies produces a waveform that is a high-frequency “carrier wave” (corresponding to the average of the frequencies of the two sinusoids) modulated by a slow envelope oscillating at the “beat” frequency. This slow envelope is able to successfully engage neurons. At locations where the amplitude of one sinusoid dominates the other (e.g. closer to one of the electrodes), the envelope does not oscillate significantly, and the neurons are observed to not fire.

Note that if the strategy was simply utilizing the low-pass filtering effect of the neural membrane [12], then it would not engage neurons at all because a low-pass filtering of a superposition of two high-frequency sinusoids would (ideally) yield a zero output. Fundamentally, the strategy must exploit a *nonlinearity* in the membrane potential dynamics to do some sort of envelope demodulation. Interestingly, studies [13], [14] have noted a form of nonlinearity, namely, rectification, that is relevant to *nonideal* envelope demodulation. Our observations suggest that indeed, it is the non-ideal envelope demodulation that the neurons are performing.

Limitations of the strategy employed in Grossman *et al.*: TI stimulation is promising, but has important limitations: to not stimulate neurons along the plane equidistant from the two electrode-pairs (see the $x = 0$ plane in Fig. 9a), the technique depends solely on current dispersion patterns, and placement of the electrodes. Along the z -axis, the strategy requires currents to concentrate quickly as they get shallower. However, for large heads with thick skulls, current disperses significantly as it leaves the skull and enters the brain (analogous to dispersion of EEG signals [15], [16]). Consequently, currents are less concentrated in shallow regions, reducing the spatial precision substantially. Along the y -axis, where the amplitudes of the two sinusoids are equal, the technique requires the activating function to decay quickly to limit the region of

stimulation. Again, for media in which current has dispersed significantly before entering the brain, this may not occur, leading to a large stimulated region.

Conventionally, transcranial Direct Current and Alternating Current Stimulation (tDCS and tACS, respectively) tend to have poor focusing precision. Carefully chosen electrode montages near regions of interest are capable of generating more focused stimulation [17], [18], [19]. Another class of strategies use a larger number of electrodes (8 in [20], 64 in [21], and 336 electrodes [22]) whose locations are guided by standard [15] (“10-20”) EEG electrode locations. They then solve optimization problems to generate desired stimulation patterns. However, unlike the results in this paper, these approaches [20], [21], [22] utilize only spatial interference, and are unable to get high precision while stimulating deep sites.

Our contributions: This work addresses these critical limitations of the technique in Grossman *et al.*, and also develops techniques for *multisite* and *steerable* stimulation. Intuitively, the spatial-interference aspect of our technique is used to limit the spatial extent of stimulation along the z -axis, while we advance on the temporal-interference aspect to reduce stimulation along the x - and y -axes.

For illustrating our contributions, we utilize Hodgkin-Hodgkin-type (HH-type) neuron models, and assume a simplistic “sea-of-neuron” brain model, i.e. all the neurons are isolated, have the same orientation, and are of the same type (which is one of three types of neurons). Implicitly, our model approximates the situation where the experimenter aims to stimulate one of the neuron-types but does not care whether others are stimulated or not. If other situations are desired, e.g. stimulating one but not others, it is plausible that the strategies can be adapted. The assumption of homogeneous neural orientation only leads us to underestimate the precision of our strategies because it disallows us from exploiting orientation diversity (see Section II-A). This model is carefully chosen to have the needed simplicity so insights can be gained and tested, and yet rigor so that novel strategies designed using the model are relevant in the real world. We start with the classical squid giant axon model [8], and then use a mammalian excitatory neuron from [23]. For a third neuron-type, we use an inhibitory mammalian parvalbumin-expressing (PV) neuron [10], [11], but observe that it does not exhibit TI stimulation, and hence may not be a good candidate for TI and improved strategies². We now describe steps that help us attain increased spatial precision for the first two neuron-types:

(i) *Modeling and qualitatively recovering results of Grossman *et al.* in a computational model.* Using the HH-type models [8], [23] and simplified models of spatial dispersion of currents in tissue, we are able to obtain stimulation patterns qualitatively similar to Grossman *et al.*’s [5], which opens the door to use of computational strategies in examining and improving TI-stimulation. However, only some neuron-types appear to exhibit TI stimulation.

²Our understanding is that it might be difficult to control stimulation of PV neurons while using our strategies to stimulate excitatory or HH-squid neurons, but this needs to be understood using subsequent and more complex models.

(ii) *Multielectrode TI stimulation.* Using the classical HH model, we observe that very low frequency TI envelope modulations require higher values of activating function for stimulation (see Fig. 5). This observation leads us to propose novel multielectrode TI strategies that attain higher precision stimulation than the 2-electrode-pair strategies in Grossman *et al.* [5]. Our strategies involve having small differences in frequencies in nearby electrode-pairs, and larger differences in frequencies in farther electrode-pairs. We show in Fig. 8b and Fig. 9b that when using 16 electrode-pairs, shallow stimulation in the $z = 0.4$ -plane (the stimulation is expected to happen at $[0, 0, 0.4]$) is indeed suppressed compared to the original 2-electrode-pair TI stimulation.

(iii) *STIMULUS*, which goes a step further and harnesses spatial diversity to generate “current lenses” that focus a particular set of activating functions at desired points. One can think of this strategy as replacing an electrode-pair in multielectrode TI with a “patch-pair” consisting of multiple electrode-pairs, with each electrode-pair in the same patch-pair generating currents of the same frequency. These patch-pairs act as current lenses, and the combined effect of these lenses improves resolution of multielectrode TI. We generate spatial interference patterns by exploiting knowledge of decay of currents in tissue to focus the signal of each patch-pair near the desired site of stimulation. This is an adaptation of the concept of “beamforming” in spatial filtering [24], [20], [21] to the case where multiple beamforming patches are used.

Finally, in Section III, we also show that STIMULUS can obtain dynamic steerability of stimulation (without moving the electrodes themselves), and can obtain simultaneous stimulation at multiple sites, providing rich patterns of stimulation. Steerable multisite stimulation is important in many applications, e.g. in providing feedback in brain-machine interfaces, and in peripheral nerve stimulation [25], [26].

II. METHODS

A. 3D head model based on FEM and Hodgkin-Huxley equations

We use a 4-sphere head model [16], consisting of brain, cerebrospinal fluid (CSF), skull, and scalp layers. To simulate different head sizes across species and ages, we allow the outermost radius i.e. the outer surface of the scalp layer to vary, while the ratios of the radii (calculated using those of human head, namely 7.5 cm, 7.9 cm, 8.6 cm and 9.2 cm for the 4 spheres [16]) are kept constant consistent. The outermost radius is assumed to be 10 cm for easier interpretability of the results. Current dispersion is modeled through a finite-element method (FEM) that incorporates conductances in each layer, and boundary conditions are provided by input currents from the electrodes. We assume a purely resistive medium for current dispersion, as has been reported at least for frequencies of a few hundred Hz [27] (see Section IV).

The head model is discretized by intersecting the head, i.e., a 10 cm-radius sphere, with a three-dimensional orthogonal lattice (x -, y -, and z -axis spacings being 0.4 cm), whose neighboring vertices are connected by resistors. Note that while tetrahedral meshes can be used [17], for simplicity of

calculating z -directional current gradients, we use a hexahedral (i.e. with cubic elements) mesh, which is also commonly adopted [28]. We define a “voxel” as a cube centered at a node in the lattice, whose faces bisect the lines connecting the node and its nearest neighbors, and are perpendicular to the lines. Values of these resistors are based on which layer of the head they are in. Value from the outer layer is used when a resistor connects two different layers. Voltages, as well as their spatial second derivatives at each node, are then obtained by utilizing Kirchhoff’s current law and the boundary conditions on the currents.

For modeling neural response to these external inputs, we use the well known Hodgkin-Huxley-type (HH-type) models [8], [23]. While the original model, which is commonly adopted by neurostimulation papers [21], [17], [5], assumes that neural stimulation is driven by the *amplitude* of the current external to the neuron, we here adopt a well-accepted model, where the neuron responds to the “activating function” of the external current [29], [30]. Indeed, there is experimental evidence demonstrating that it is activating functions that play a role in neuronal stimulation [31]. This activating function is proportional to the spatial second derivative of voltage along the axon. Formally, the activating function is defined as $\frac{a}{2R} \frac{\partial^2 V}{\partial z^2} = \frac{a}{2R} V_{zz}$, where a is the radius of the neuronal axon, R is the resistivity of intracellular fluid, z is the axonal direction, and V_{zz} is simply a notation for the second spatial derivative in the z -direction. The second spatial derivative can be calculated using Eq. (7) in [29]. Note that the spatial second derivative of voltage is proportional the spatial first derivative of current [29], [32]. In order to evaluate the improvement using our proposed strategies, we use both the classical squid giant axon model [8], as well as the mammalian excitatory pyramidal neuron in [23]. When testing the influence of neuron-type on TI, the PV neuron³ in [10], [11] is also used.

For simplicity, we assume that we know the axonal orientation of the neuron to be stimulated, and that all neurons in the brain are described by the same Hodgkin-Huxley parameters and the same orientation (along the z -axis). Because all neurons are assumed to be oriented along the z -axis, only z -directional activating functions are computed, and the computation is performed at all voxels in the head model. The resulting distribution of second derivatives of voltage is illustrated in Fig. 1.

B. Defining firing events

For each simulation, we solve Hodgkin-Huxley equations using the Dormand-Prince method [33] for a total span of 1000 ms sampled at 25 kHz. In order to estimate firing, we apply a sixth-order Butterworth bandpass filter to keep only frequency components between 100 and 1000 Hz [5]. We adopt a simple criterion to decide firing: when the filtered membrane potential crosses a threshold, we deem it as a firing event. This was checked visually for all neuron-types. To avoid boundary effects in time (start and end of stimulation), we removed the first and last parts of the time trace of the

³We had a personal communication [11] with the authors of [10] for a parameter correction in the model.

potential. For the classical HH neuron, we choose the threshold to be 30 mV, and for the excitatory neuron, the threshold is chosen to be 2 mV. Such thresholds are empirically observed to obtain robust firing (see Fig. 3 and Fig. 7) in the neuron model. There are cases when the membrane potentials show a tendency to fire by having small peaks in the filtered response, yet the peaks are not pronounced enough for us to classify them as firing.

C. STIMULUS optimization problem for each patch-pair

We now formally describe how these constraints of constructive and destructive interference are formulated as an optimization problem for each patch-pair. We use bold font to denote vectors, and uppercase bold font to denote matrices. For any matrix \mathbf{A} , \mathbf{A}^T denotes its transpose. Assume that we have p electrode-pairs in each patch-pair with current-amplitudes $\mathbf{x} = [x_1, x_2, \dots, x_p]^T$. Let us assume that there are n focus points for this patch-pair, and m points where we minimize activating functions to suppress stimulation.

Let us define **activating function decay (AFD) factor** as the ratio of the generated activating function value at a point to the total input current from an electrode-pair that generates the current distribution. Thus, this factor depends both on the location of the point at which the activating function (due to just the chosen electrode-pair) is being estimated, and the location of the electrode-pair generating currents. Note that the AFD factors also depend on the head-radius and all the parameters in the 4-sphere model we use, but the dependence is implicit in our notation. Let $\mathbf{A}_{\text{focus}}$ and $\mathbf{A}_{\text{cancel}}$ denote the AFD-factor matrices, formed by the focus and cancellation points respectively, where $\mathbf{A}_{\text{focus}}$ is a $p \times n$ matrix and $\mathbf{A}_{\text{cancel}}$ is a $p \times m$ matrix with each column being a vector containing the AFD factors from all electrodes to a focus point (for $\mathbf{A}_{\text{focus}}$) or a cancel point (for $\mathbf{A}_{\text{cancel}}$). Therefore, the total activating function at focus points can be written as $\mathbf{A}_{\text{focus}}^T \mathbf{x}$, and at cancel points, $\mathbf{A}_{\text{cancel}}^T \mathbf{x}$.

For computational tractability, we formulate our objective function as minimization of the square sum of activating functions at all cancel points, $\|\mathbf{A}_{\text{cancel}}^T \mathbf{x}\|^2 = \mathbf{x}^T \mathbf{Q} \mathbf{x}$ where $\mathbf{Q} = \mathbf{A}_{\text{cancel}} \mathbf{A}_{\text{cancel}}^T$.

For simplicity, we constrain the optimization problem to have each patch-pair produce the same activating function value $V_{zz,stim}$ at all focus points. The value of $V_{zz,stim}$ for optimization is the required value of activating function obtained through Hodgkin-Huxley simulations for TI waveforms that stimulate neurons in the targeted region. More precisely, for an input that is a sum of sinusoidal currents, with currents generated by the same patch-pair having the same frequency, and each patch-pair resulting in the same activating function at all stimulation foci, we empirically find the minimum amplitude $V_{zz,stim}$ of these activating functions that ensures robust stimulation in the entire targeted region.

This leads us to the following optimization problem that yields the optimal current allocation \mathbf{x}^* at each electrode-pair in a patch-pair:

STIMULUS optimization for each patch-pair:

$$\begin{aligned} \mathbf{x}^* &= \arg \min_{\mathbf{x}} \mathbf{x}^T \mathbf{Q} \mathbf{x} \\ \text{s.t. } \mathbf{A}_{\text{focus}}^T \mathbf{x} &= V_{zz,stim} \mathbf{1}, \end{aligned} \quad (1)$$

where $\mathbf{1}$ is the all-ones vector with length of number of foci, and $\arg \min_x f(x)$ denotes the operation of finding the value of x which minimizes $f(x)$. Essentially, the first line defines the problem of minimizing activation functions at the chosen locations, and the second line imposes the constraint that all foci should have equal total activating function of $V_{zz,stim}$. This problem is formulated in a manner so it is convex. Thus, finding the (unique) optimum is low complexity.

The solution of (1) provides the current allocation for each electrode-pair in a single patch-pair. Solving this equation for all patch-pairs yields current allocations for all electrode-pairs. The optimization problem is solved in MATLAB (The MathWorks, Inc., MA) using the interior-point method. The code is available at <https://github.com/JiamingCao/STIMULUS>.

III. RESULTS

A. Modeling of current distribution in the head

We use both Cartesian (x, y, z) and spherical coordinates (r, θ, ϕ) , where θ is the polar angle and ϕ is the azimuthal angle. We denote the brain's conductivity by σ_1 , CSF's by σ_2 , the skull's by σ_3 , and the scalp's by σ_4 . We assume that $\sigma_1 = \sigma_2 = \sigma_4$, and that the ratio σ_3/σ_1 is 1/15 [34] (while there is debate in the literature on this value, results for $\sigma_3/\sigma_1 = 1/80$ [15] are qualitatively similar, as illustrated in the Appendix). In the case of human head, 1 unit length corresponds to 10 cm. Nevertheless, our conclusions generalize easily to any head radius, as long as the ratios of the radii of the four layers are kept the same (because changing the radius of the head scales all the activating functions by the same constant). Therefore, for consideration of generality, in all the following figures, all Cartesian coordinates are normalized by the head-radius.

For simplicity, for all strategies, all electrode-pairs are assumed to be placed so that the line joining the electrodes is parallel to the polar axis (i.e. the z -axis). The activating function map for a single pair of electrodes in this model is shown in Fig. 1. For multiple electrode-pairs, the overall extracellular stimulating current is simply the sum of extracellular currents due to individual electrode-pairs. The induced current inside the neuron is simply the activating function, that is, the first spatial derivative of the current (appropriately scaled), applied to this overall current. In this paper, we are not explicitly considering the scaling constant (i.e. $a/2R$). Because all neurons are assumed to be of the same type and orientation, such constant only scales the activating function at all neurons by the same constant.

B. Understanding 2-electrode-pair TI stimulation using computational models

Before describing our multielectrode TI stimulation and STIMULUS strategies, we first observe using the classical HH

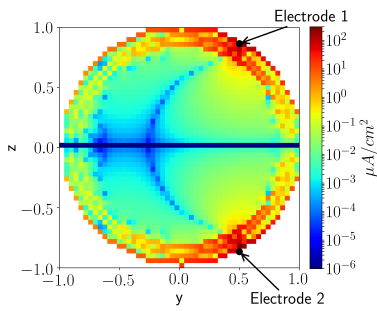


Fig. 1. Distribution of activating function as a result of a single electrode-pair. Assume that the input current is $1 \mu\text{A}$, the outer radius of the head is 1 cm , and $\sigma_1 = 1 \text{ S}$. The electrode in the upper hemisphere is placed at $\theta = \pi/6$, and $\phi = 0$. The distribution of actual activating functions is proportional to the values shown in this figure (see Section II-A).

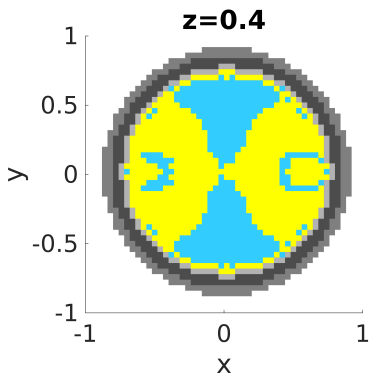


Fig. 2. TI does not work with the classical HH neuron when the base frequency is not high enough. In this example, the frequencies are chosen to be 1200 and 1250 Hz , and the activating function generated by each electrode-pair is $57 \mu\text{A}/\text{cm}^2$ at $[0,0,0.4]$. Stimulation does not stop when moving away from center towards the electrodes. Result is shown as a slice at the $z = 0.4$ -plane. Blue: no stimulation; Yellow: stimulation; Gray layers from outside to inside: scalp, skull, and CSF.

squid neuron that the *in vivo* results of [5] can be replicated using our computational model. This provides an improved understanding of how neurons respond to envelope waveforms and base frequencies of interfering waveforms.

Using our model, we first observe that TI stimulation fails at low base frequencies, e.g. 300 Hz or even up to 1500 Hz . In order to stimulate the target region, these base frequencies produce substantial undesirable stimulation at locations far from the target as well. Fig. 2 shows that for the classical HH squid neuron, when the base frequency is not high enough (1200 Hz in this case), even though the center of the plane where the two sinusoids generate equal amplitudes is only barely stimulated, the total stimulated region connects the center point to the brain surface close to the electrodes. It seems that neurons can still follow these slower base frequencies.

In contrast, at base frequencies larger than 2000 Hz , we observed that these neurons exhibit TI stimulation in that neural firing is observed to stop as one moves away from sites with equal amplitude of the sinusoidal currents. Fig. 3 shows that for the classical HH squid neuron with two electrode-

pairs operating at frequencies 2000 Hz and 2050 Hz , results are qualitatively consistent with those in [5].

On the z -axis, where both sinusoidal currents have equal amplitude (Fig. 3a), robust firing is observed, as can be inferred from bandpass filtered membrane potential. If we probe a neuron far from center (e.g. in Fig. 3c), the currents have unequal amplitudes and the envelope has less “depth” in its “valleys”. The filtered membrane potential shows that the firing stops in this case. This observation fully agrees with those reported in Grossman *et al.* For the chosen location in Fig. 3b, the probed neuron lies in between the above two. Here, the envelope has a larger (but not large enough) difference between peaks and valleys, and from the filtered membrane potential, it appears as if the neuron is close to firing, but does not fire. The membrane potential has some high frequency components, but the amplitudes are small.

To quantify our improvements, we assume for most of our initial (single, fixed focus) results that the target stimulation region contains $[0,0,0.4]$, which is deeper than half of the brain and hence sufficient to examine the capability of deep-brain stimulation. Further, we impose the constraint that the stimulation pattern includes a “disk” of diameter approximately 2 cm around the center of the target region. This is motivated by the observation that in deep-brain stimulation, one may be interested in stimulating only a deep region in the brain (e.g. the hippocampus, but not the tail of caudate nucleus which is just above the hippocampus). More importantly, it forces all stimulation strategies to stimulate a minimal region, not just a single point. The latter can yield unrealistically optimistic results and strategies may not work in practice because, theoretically, optimization strategies can tailor current waveforms to only barely stimulate the targeted single point in the space, but in practice, small uncertainty/variability in conductivity parameters or neural parameters can render these strategies ineffective.

The resulting stimulation using 2-electrode-pair TI with classical HH neurons is shown in Fig. 8a along the planes $x = 0$, $y = 0$, and $z = 0.4$. For any one electrode-pair, one electrode is placed at $\theta = \pi/6$ and the other at $\theta = 5\pi/6$ on the $y = 0$ plane. The azimuths of the two electrode-pairs are chosen to be $\phi = 0$ and $\phi = \pi$, and the frequencies assigned to them are 2000 and 2050 Hz respectively. Both electrode-pairs are required to provide the same activating function at the center of the target region, and the value is chosen to be $185 \mu\text{A}/\text{cm}^2$ for each of the electrode-pairs. Note that undesirable shallow stimulation is observed in conjunction with deeper stimulation.

In Fig. 9a, we illustrate that for the excitatory pyramidal neuron, a similar replication of the experimental results in [5] can also be achieved. The placement of electrodes are the same as in the case of using the classical HH neuron. The frequencies of the the two electrode-pairs are chosen to be 2500 and 2515 Hz , and each of them is required to generate an activating function of $440 \mu\text{A}/\text{cm}^2$ at the center of the target region (i.e. $[0,0,0.4]$). We observe that for either of the neuron-types, it is infeasible to cover the whole 2 cm disk, even when amplitudes of the input currents are significantly increased. This is because activation function decays fast when

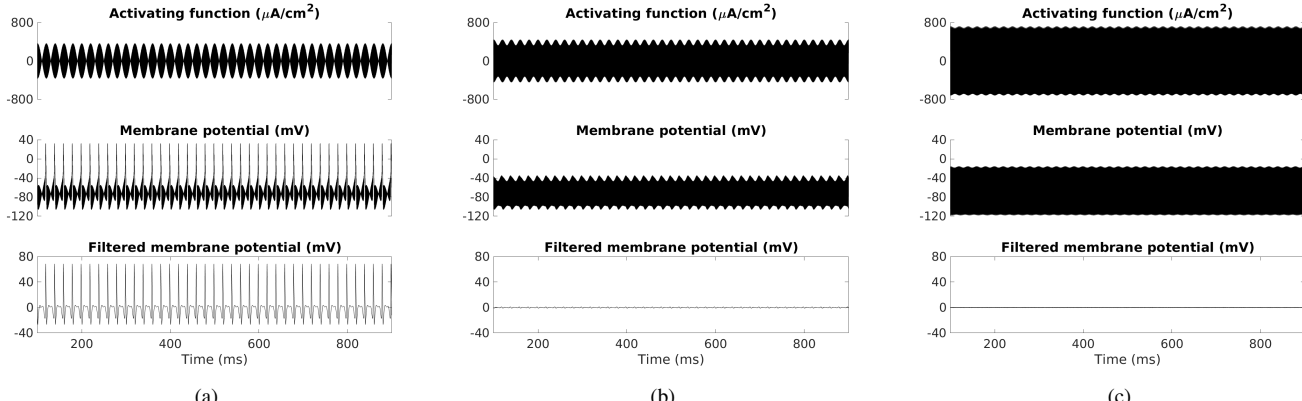


Fig. 3. Activating functions, membrane potentials, and filtered membrane potentials (filtered between 100 and 1000 Hz to visualize firing) of neurons at different locations using classical HH model and 2 electrode-pairs. (a) Waveforms at the center of the target region ($[0, 0, 0.4]$), where both sinusoidal currents have equal amplitudes. The envelope touches 0, and hence has the maximum modulation depth. Clear evidence of neuron firing is seen in the filtered membrane potential. (b) Waveforms at a point slightly away from the center of the target region ($[0.08, 0, 0.4]$), where amplitudes of the two sinusoids are slightly different, and the envelope does not reach zero. Filtered membrane potential reveals that the neuron is close to firing, but the potential does not exceed the 30 mV threshold, and thus is not considered to be firing. (c) A point farther away from the target region ($[0.16, 0, 0.4]$), where the two sinusoids have substantially different amplitudes, causing the envelope to be rather flat and far from zero. The neuron does not show any evidence or tendency of firing.

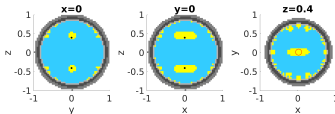


Fig. 4. PV neurons do not exhibit TI stimulation. Electrode configuration and target are chosen to be the same as in Fig. 9a, and firing pattern on the $z = 0.4$ -plane is shown. Base frequency is increased to 4000 Hz. While firing stops when moving close the electrodes, neurons near the two diagonals are heavily engaged.

moving away from the electrodes, such that modulation depth of the envelope quickly decreases when moving from the z -axis towards the electrodes and therefore stops stimulation.

Do all neuron-types exhibit TI stimulation?: We tested the strategy with another type of mammalian neuron, namely parvalbumin-expressing (PV) neurons (parameters drawn from [10], [11]). The electrode placement and desired focus are kept the same as in previous TI stimulation results. We choose to stimulate only the center voxel of the target region, in order to estimate the minimum possible excess stimulation. We swept base frequencies across a large range (a few hundred hertz to 4000 Hz) to allow the neuron-type to exhibit TI at any base frequency. Simulations reveal that (see Fig. 4), even when using a base frequency of as high as 4000 Hz, voxels near the lines that are 45° from the line joining two electrode-pairs are engaged, though neurons close to the electrodes do not fire. The activating function generated by each electrode-pair is chosen to be $307 \mu\text{A}/\text{cm}^2$ at the center of the target region, which is the minimal value that stimulates only the center voxel. The frequencies are chosen to be 4000 and 4015 Hz . This result suggests that with PV neurons, it is not possible to perform deep brain stimulation non-invasively using TI stimulation.

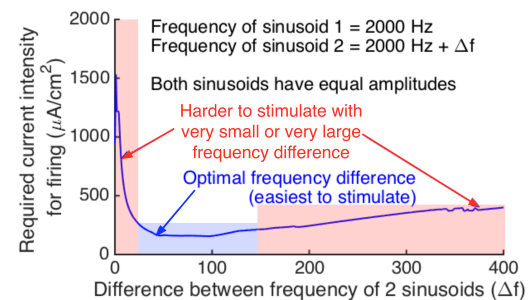


Fig. 5. Minimum activating function of envelope-modulated signal needed for 2-electrode TI stimulation for the classical HH neuron. Frequency of the slower sinusoid is fixed at 2000 Hz. The figure shows that there is an optimal frequency difference of the interfering sinusoids (both of equal amplitude) to enable stimulation at values of activating function. We utilize this observation in the design of our multielectrode TI strategy.

C. Improving spatial precision using multielectrode TI stimulation

To extend TI stimulation to more than 2 electrode-pairs and improve its spatial precision, let us first use the classical Hodgkin-Huxley squid neuron to obtain a deeper understanding of the 2-electrode-pair TI stimulation [5] as we vary stimulation parameters. Focusing on two equal-amplitude interfering sinusoidal currents, one at 2000 Hz and the other at $(2000 + \Delta f)$ Hz, and vary Δf , Fig. 5 shows that the threshold activating function needed to achieve effective TI stimulation is higher when the difference in frequencies is smaller. For 2-electrode-pair TI configuration, the smallest required current density is at $\Delta f = 30$ to 40 Hz , and hence the neurons are easiest to stimulate at that frequency difference.

More importantly, the required current amplitudes to stimulate rise steeply as Δf is lowered below 10 Hz. This observation suggests an interesting strategy for frequency allocation and electrode-pair placement for multielectrode TI stimulation. First, for electrode placement, we place electrode-pairs as

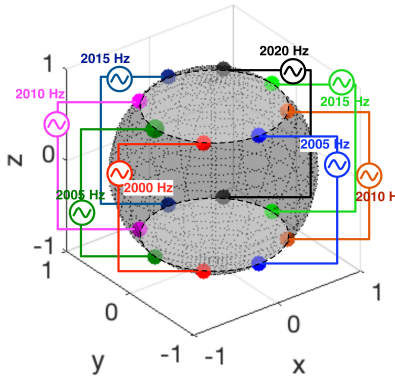


Fig. 6. Example placement of electrode-pairs. For each electrode-pair, the electrodes are symmetric about the $z = 0$ -plane, and the electrode-pairs are arranged evenly in a ring fashion on the sphere.

shown in Fig. 6: each electrode-pair has exactly one electrode in the top hemisphere, and the electrodes in the top hemisphere are arranged in a ring. Electrodes in the bottom hemisphere and their top hemisphere counterparts are symmetric about the $z = 0$ -plane. We note that although the electrode-pair arrangement used here is specified for spherical head models, in cases of real heads it is still possible to approximate such a ring arrangement with the focus of stimulation on the axis of the ring.

Next, we discuss frequency allocation for the electrode-pair placement discussed above. The goal is to have the neurons away from the target region to not fire while having the neurons within fire. If one allocates frequencies so that nearby electrode-pairs have frequencies close to each other (e.g. 1-5 Hz), but diametrically opposite electrode-pairs can have large differences (e.g. up to 30 Hz), then away from the center, the dominant sinusoids have frequencies close to each other, lowering the higher-frequency-content (~ 30 Hz) of the envelope, which makes firing less likely to happen. However, close to the center of the target region, because all sinusoids are adding up with approximately equal amplitudes, the envelope can have significant high frequency content. Analogous to 2-electrode-pair TI (Fig. 3), we illustrate the classical Hodgkin-Huxley neuron responses at different spatial locations for 16-electrode-pair TI in Fig. 7. To quantify the improvements, the target region is still chosen to be a 2 cm disk at $[0,0,0.4]$. The observation of [5] can now be generalized to more complicated envelopes: stimulation is more likely to happen when the envelope is less flat, and the interfering sinusoids have almost equal amplitudes.

Indeed, this strategy succeeds in outperforming 2-electrode-pair TI with reduced shallow stimulation in the $z = 0.4$ -plane, as shown in Fig. 8b. The same improvement is also seen with the excitatory pyramidal neurons, as is shown in Fig. 9b. Details of electrode configurations used in the simulations above can be found in Table I.

However, it is not hard to notice that the stimulation pattern still fails to fully cover the desired region, and that close to the skull, undesired stimulation is still existent. Moreover, because this strategy does not *actively* limit the spread of stimulation

Neuron-type	Classic HH	Excitatory
Azimuthal locations	$0, \pi/8, \pi/4, \dots, 15\pi/8$	
Polar locations	$\pi/6, 5\pi/6$ (upper, lower)	
Target	$[0,0,0.4]$	
Frequencies (Hz)	2000, 2005, 2010, 2015, 2020, 2015, 2010, 2005, 2000, 1995, 1990, 1985, 1980, 1985, 1990, 1995	2500.00, 2501.25, 2502.50, 2503.75, 2505.00, 2503.75, 2502.50, 2501.25, 2500.00, 2498.75, 2497.50, 2496.25, 2495.00, 2496.25, 2497.50, 2498.75
$V_{zz,stim}$ per pair ($\mu A/cm^2$)	44	70

TABLE I
PARAMETERS USED IN DEMONSTRATION OF MULTIELECTRODE TI STIMULATION.

region, in certain cases (e.g. thicker skull) the stimulation region can potentially become undesirably extended.

It is possible that further increase in number of electrodes using multielectrode TI stimulation could further suppress shallow engagement of neurons and achieve precision, but, extrapolating from Fig. 8b, it would likely come at the cost of reduced firing rate. We now describe how STIMULUS exploits spatial diversity and combines beamforming approaches with TI strategies to achieve stimulation with high spatial precision.

D. Harnessing spatial diversity using STIMULUS

In the electrode-pair configurations in the 2-electrode-pair TI [5] and multielectrode TI stimulation strategies above, the focus as well as spatial extent of stimulation depends only on the electrode placement and current dispersion in the brain. This means that we are not able to actively control the precision of stimulation, and can potentially create unacceptably extended stimulation regions.

Here, we propose our alternative strategy – STIMULUS – that generates spatio-temporal patterns of interference to improve spatial resolution. Intuitively, one can think of this strategy as replacing an electrode-pair in multielectrode TI stimulation with a “patch-pair” constituted by multiple electrode-pairs, with each electrode-pair in each patch-pair generating currents of the same frequency. It is instructive to think of each patch-pair of electrodes as a “computational current lens”, that attempts to focus activating functions (using constructive interference) at some desired points of focus, and cancel activating functions (using destructive interference) at a few other (carefully chosen) points.

We quantify the improvement of precision using STIMULUS. We observe that for both the classical HH neuron and the excitatory pyramidal neuron, the resulting stimulation covers the desired target region, and shallow engagement is significantly reduced compared to both 2-electrode-pair and multielectrode TI stimulation, as is shown in Fig. 8c and Fig. 9c for the two neuron-types respectively. In order to obtain this result for the classical HH neuron, we use 8 patch-pairs, whose centers are placed azimuthally using the same strategy as in multielectrode TI stimulation (see Fig. 6), and they all span for an angular azimuthal range of $\pi/4$. In the polar direction, patches in the top hemisphere all span from $\theta = \pi/12$ (i.e. $\pi/12$ from the pole) to the equator, with

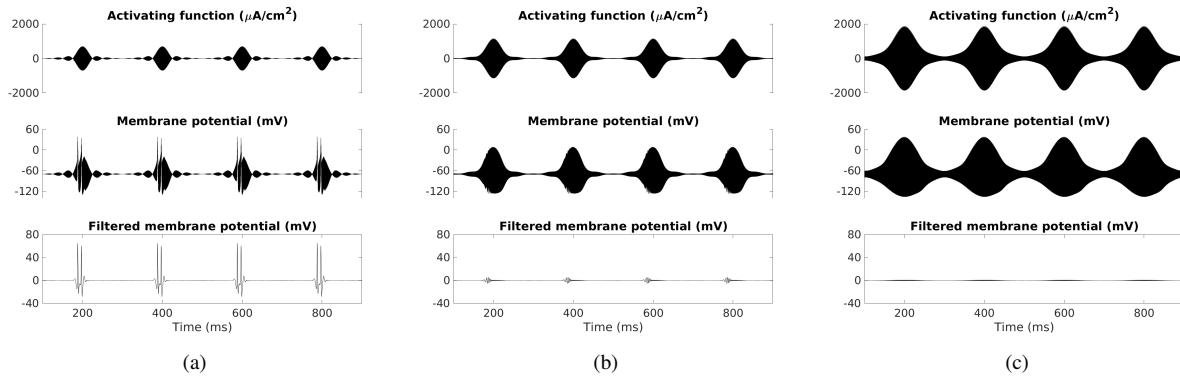


Fig. 7. Activating functions, membrane potentials, and filtered membrane potentials (filtered between 100 and 1000 Hz to visualize firing) of neurons at different locations. (a) Waveforms at the center of the target region ($[0,0,0.4]$), where all sine waves have equal amplitudes. Clear evidence of neural firing is present. (b) Waveforms at a point slightly away from target region ($[0.24,0,0.4]$), where the amplitudes of the interfering sinusoids are slightly different. Membrane potentials show that the neuron has a tendency to fire, but does not fire. (c) Waveforms at a point farther away from the target region ($[0.6,0,0.4]$), where the interfering sinusoidal currents have very different amplitudes. The neuron does not show any evidence or tendency of firing.

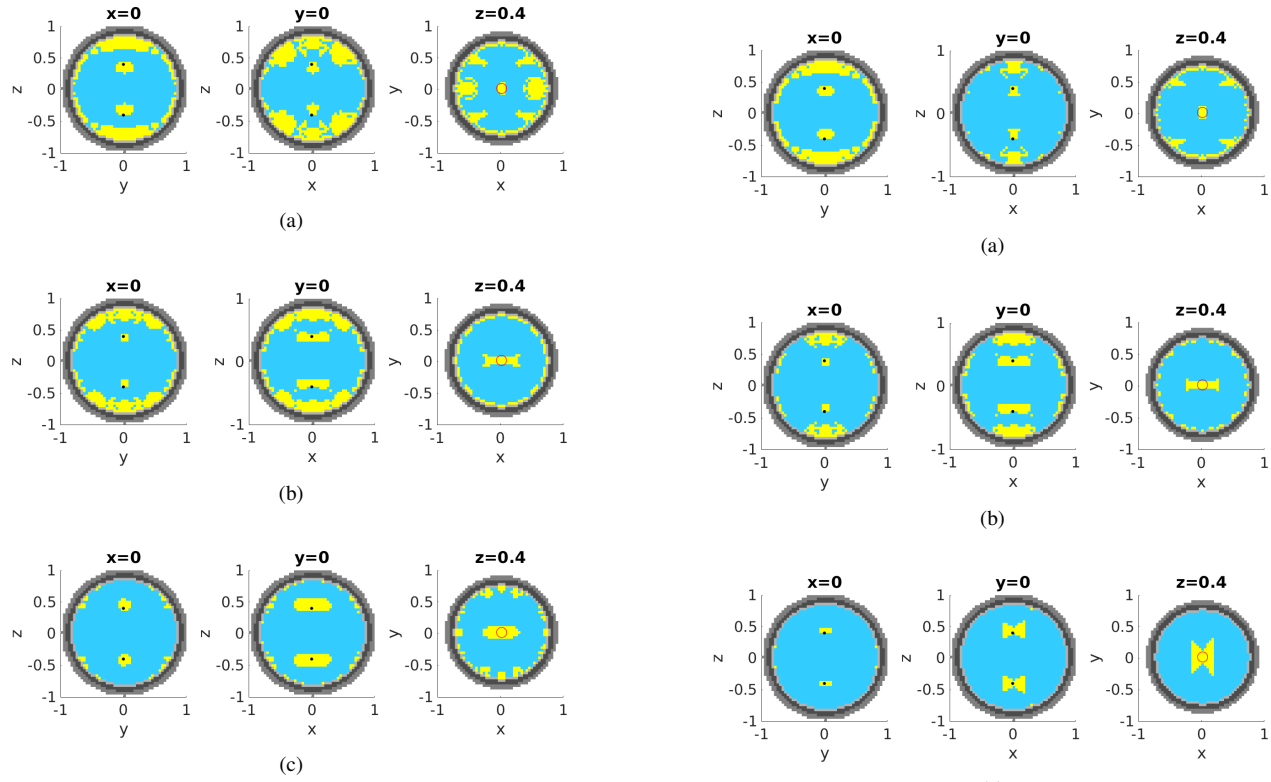


Fig. 8. Stimulation regions using TI stimulation, multielectrode TI stimulation, and STIMULUS. Classical HH model [8] is used. Center of target region is $[0,0,0.4]$ for all strategies. (a) TI stimulation of Grossman *et al.*, which uses 2 pairs of electrodes in the $y = 0$ plane, fails to cover the total desired region of a disc with 2 cm diameter, and causes a large amount of shallow neurons to be engaged; (b) Multielectrode TI using 16 pairs of electrodes provides an improved precision by reducing shallow stimulation, but the reduction is limited and it is still difficult to cover the desired region; (c) STIMULUS using 8 patch-pairs causes only minimal shallow engagement, and covers the target region, attaining a high precision of stimulation. Blue: no stimulation; Yellow: stimulation; Gray layers from outside to inside: scalp, skull, and CSF. Focus points are indicated by black dots, and target regions are indicated by red circles.

Fig. 9. Stimulation regions using TI stimulation, multielectrode TI stimulation, and STIMULUS. Excitatory cortical pyramidal model [23] is used. Center of target region is $[0,0,0.4]$ for all strategies. (a) 2-electrode-pair TI stimulation fails to cover the desired target region, and causes a large amount of shallow stimulation; (b) 16-electrode-pair TI stimulation reduces shallow stimulation, but still fails to cover the target region; (c) STIMULUS using 2 patch-pairs causes only minimal shallow engagement, and covers the target region, attaining a high precision of stimulation. Blue: no stimulation; Yellow: stimulation; Gray layers from outside to inside: scalp, skull, and CSF. Focus points are indicated by black dots, and target regions are indicated by red circles.

Number of patches	8								
Electrodes per patch	300								
Azimuthal centers	$0, \pi/4, \pi/2, 3\pi/4, \pi, 5\pi/4, 3\pi/2, 7\pi/4$								
Azimuthal width	$\pi/4$								
Polar span ([min θ , max θ])	$[\pi/12, \pi/2]$								
Frequencies (Hz)	2000, 2007.5, 2015, 2007.5, 2000, -1992.5, -1985, -1992.5								
Single deep focus	<table border="1"> <tr> <td>Focus</td> <td>[0,0,0.4]</td> </tr> <tr> <td>Cancel</td> <td>[0,0,0.52]</td> </tr> <tr> <td>Max. current per pair (μA)</td> <td>60</td> </tr> <tr> <td>$V_{zz,stim} (\mu A/cm^2)$</td> <td>109</td> </tr> </table>	Focus	[0,0,0.4]	Cancel	[0,0,0.52]	Max. current per pair (μA)	60	$V_{zz,stim} (\mu A/cm^2)$	109
Focus	[0,0,0.4]								
Cancel	[0,0,0.52]								
Max. current per pair (μA)	60								
$V_{zz,stim} (\mu A/cm^2)$	109								
Single shallow focus	<table border="1"> <tr> <td>Focus</td> <td>[0,0,0.6]</td> </tr> <tr> <td>Cancel</td> <td>[0,0,0.48], [0,0,0.72]</td> </tr> <tr> <td>Max. current per pair (μA)</td> <td>60</td> </tr> <tr> <td>$V_{zz,stim} (\mu A/cm^2)$</td> <td>109</td> </tr> </table>	Focus	[0,0,0.6]	Cancel	[0,0,0.48], [0,0,0.72]	Max. current per pair (μA)	60	$V_{zz,stim} (\mu A/cm^2)$	109
Focus	[0,0,0.6]								
Cancel	[0,0,0.48], [0,0,0.72]								
Max. current per pair (μA)	60								
$V_{zz,stim} (\mu A/cm^2)$	109								
Multisite	<table border="1"> <tr> <td>Focus</td> <td>[0,0,0.48], [0,0,0.76]</td> </tr> <tr> <td>Cancel</td> <td>[0,0,0.64]</td> </tr> <tr> <td>Max. current per pair (μA)</td> <td>65</td> </tr> <tr> <td>$V_{zz,stim} (\mu A/cm^2)$</td> <td>113</td> </tr> </table>	Focus	[0,0,0.48], [0,0,0.76]	Cancel	[0,0,0.64]	Max. current per pair (μA)	65	$V_{zz,stim} (\mu A/cm^2)$	113
Focus	[0,0,0.48], [0,0,0.76]								
Cancel	[0,0,0.64]								
Max. current per pair (μA)	65								
$V_{zz,stim} (\mu A/cm^2)$	113								

TABLE II

PARAMETERS USED FOR THE CLASSICAL HH NEURON IN DEMONSTRATION OF STIMULUS. NOTE THAT THE MAXIMUM CURRENT PER ELECTRODE-PAIR IS CALCULATED USING A 10 CM HEAD-RADIUS, AND IS SUBJECT TO A INDIVIDUAL-DEPENDENT CONSTANT (SEE SECTION II-A).

Number of patches	2								
Electrodes per patch	200								
Azimuthal centers	$0, \pi$								
Azimuthal width	$\pi/5$								
Polar span ([min θ , max θ])	$[\pi/12, \pi/2]$								
Frequencies (Hz)	2500, 2515								
Single deep focus	<table border="1"> <tr> <td>Focus</td> <td>[0,0,0.4]</td> </tr> <tr> <td>Cancel</td> <td>[0,0,0.52]</td> </tr> <tr> <td>Max. current per pair (μA)</td> <td>100</td> </tr> <tr> <td>$V_{zz,stim} (\mu A/cm^2)$</td> <td>420</td> </tr> </table>	Focus	[0,0,0.4]	Cancel	[0,0,0.52]	Max. current per pair (μA)	100	$V_{zz,stim} (\mu A/cm^2)$	420
Focus	[0,0,0.4]								
Cancel	[0,0,0.52]								
Max. current per pair (μA)	100								
$V_{zz,stim} (\mu A/cm^2)$	420								
Single shallow focus	<table border="1"> <tr> <td>Focus</td> <td>[0,0,0.6]</td> </tr> <tr> <td>Cancel</td> <td>[0,0,0.48], [0,0,0.72]</td> </tr> <tr> <td>Max. current per pair (μA)</td> <td>70</td> </tr> <tr> <td>$V_{zz,stim} (\mu A/cm^2)$</td> <td>425</td> </tr> </table>	Focus	[0,0,0.6]	Cancel	[0,0,0.48], [0,0,0.72]	Max. current per pair (μA)	70	$V_{zz,stim} (\mu A/cm^2)$	425
Focus	[0,0,0.6]								
Cancel	[0,0,0.48], [0,0,0.72]								
Max. current per pair (μA)	70								
$V_{zz,stim} (\mu A/cm^2)$	425								
Multisite	<table border="1"> <tr> <td>Focus</td> <td>[0,0,0.52], [0,0,0.76]</td> </tr> <tr> <td>Cancel</td> <td>[0,0,0.6]</td> </tr> <tr> <td>Max. current per pair (μA)</td> <td>80</td> </tr> <tr> <td>$V_{zz,stim} (\mu A/cm^2)$</td> <td>435</td> </tr> </table>	Focus	[0,0,0.52], [0,0,0.76]	Cancel	[0,0,0.6]	Max. current per pair (μA)	80	$V_{zz,stim} (\mu A/cm^2)$	435
Focus	[0,0,0.52], [0,0,0.76]								
Cancel	[0,0,0.6]								
Max. current per pair (μA)	80								
$V_{zz,stim} (\mu A/cm^2)$	435								

TABLE III

PARAMETERS USED FOR THE EXCITATORY CORTICAL NEURON IN DEMONSTRATION OF STIMULUS. NOTE THAT THE MAXIMUM CURRENT PER ELECTRODE-PAIR IS CALCULATED USING A 10 CM HEAD-RADIUS, AND IS SUBJECT TO A INDIVIDUAL-DEPENDENT CONSTANT (SEE SECTION II-A).

symmetric placement (about $z = 0$ -plane) in the bottom hemisphere. For each patch in the top hemisphere, 300 electrode locations are chosen randomly within their spatial extent. For the excitatory pyramidal neuron, two patch-pairs with 200 electrode-pairs are placed in a similar manner, with locations that are randomly chosen on each of the top patches. For all the results below, placement of electrodes are kept unchanged for each neuron-type. For each simulation, all patch-pairs are required to (approximately) cancel the activating function at the same locations, and generate the same activating function at the focus points. All electrode pairs are constrained by the same maximum allowed current. Arrangement and frequency allocation of electrodes, as well as choice of parameters in the optimization problems are detailed in Table II and Table III for the classical HH neuron and excitatory cortical pyramidal neuron respectively.

Steerable and multisite stimulation: To demonstrate the steerability using STIMULUS, it suffices to show that with the same electrode locations as above, we can stimulate another target region. To do so, for both neurons, we choose to stimulate a slightly shallower region, using parameters detailed in Table II and Table III. Results for both neuron-types are shown in Fig. 10.

We further demonstrate the flexibility of STIMULUS by showing that that STIMULUS is able to stimulate two distant sites simultaneously without stimulating regions that connect the two. We still use the same placement of electrodes as for steerable stimulation above. Using parameters in Table II and Table III, we can achieve results shown in Fig. 11, demonstrating that STIMULUS can perform steerable multisite stimulation.

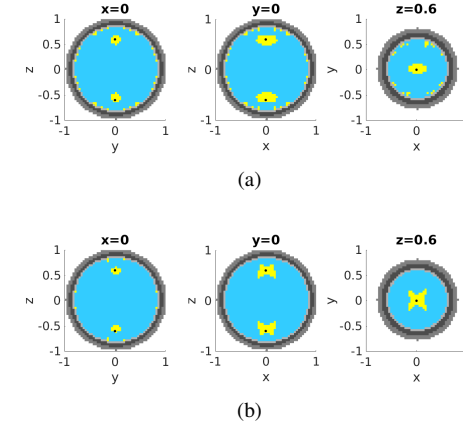


Fig. 10. Steerable stimulation: Demonstration of STIMULUS focusing at $[0, 0, 0.6]$. Notice that the slice at $z = 0.6$ is smaller because the section of the sphere in that plane has a smaller radius. Electrode placements are the same as in Fig. 8c and Fig. 9c. (a) Classical HH neuron using 8-patch-pair STIMULUS; (b) Excitatory pyramidal neuron using 2-patch-pair STIMULUS. Blue: no stimulation; Yellow: stimulation; Gray layers from outside to inside: scalp, skull, and CSF. Focus points are indicated by black dots.

IV. CONCLUSIONS AND DISCUSSIONS

We view the simplicity of our model as its strength. Our goal is to use simple models that still exhibit TI stimulation, and then develop advanced techniques using this model with associated predictions on their accuracy so they can be tested in experiments. Such close ties between theory and experiments can build confidence in the efficacy of the strategy, and speed up the adoption of the technology.

Understanding mechanisms of TI stimulation: This paper provides a novel STIMULUS strategy that creates patterns of spatiotemporal interference. Computational results suggest that this strategy can improve the precision of noninvasive neurostimulation. We also advance on the understanding of

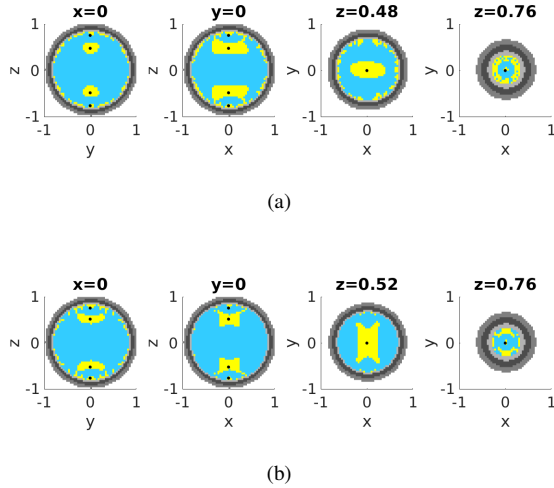


Fig. 11. Multisite steerable stimulation: Demonstration of STIMULUS focusing at two targets simultaneously. Electrode placements are the same as in Fig. 8c and Fig. 9c. Notice that the slices perpendicular to the z -axis are smaller because the sections of the sphere in that plane have smaller radii. (a) Classical HH neuron using 8-patch-pair STIMULUS, focusing at $[0,0,0.52]$ and $[0,0,0.76]$. (b) Excitatory pyramidal neuron using 2-patch-pair STIMULUS, focusing at $[0,0,0.32]$ and $[0,0,0.68]$. Blue: no stimulation; Yellow: stimulation; Gray layers from outside to inside: scalp, skull, and CSF. Focus points are indicated by black dots.

temporal interference stimulation, showing that it can be obtained in single neuron models, and extend the strategy to multiple electrodes. Obtaining TI stimulation in these models suggests that TI stimulation relies on the nonlinearity of neuronal membrane potential as a function of the external current. It also corroborates and helps understand results of [5], and prior to that, of interferential stimulation [7]. As discussed earlier, it is important to not just have experimental findings that show promise of a stimulation technique but also to understand the *mechanism* of stimulation through established (or new) biological models. Besides building confidence that the strategy indeed works, this helps optimize and extend the strategy.

We find it remarkable that TI stimulation can be observed in *single* neuron models, i.e., without taking into account the network surrounding a neuron. Network effects will certainly play a role in stimulation efficacy, but we still expect to increase the excitability of the neurons in the target region using TI stimulation, or more generally, STIMULUS.

Results in Section III suggest that the base frequency needs to be sufficiently high for a neuron to exhibit TI stimulation. We note that *this change in firing behavior as a function of base frequency suggests that the membrane potential is not simply doing an ideal envelope demodulation*. It appears that the simpler diode-resistor-capacitor-type models for a non-ideal envelope detector [35] might be better approximations. Nevertheless, the precise impact of nonlinearity of neural membrane potential as a function of the input current remains to be fully understood, and it is plausible that waveforms other than interfering sinusoids might be more effective at exploiting this nonlinearity.

Extending TI to multielectrode TI and STIMULUS: Our

computational results suggest that use of carefully designed (i.e., by studying biological mechanism of TI) multielectrode TI (16 electrode-pairs) reduces shallow stimulation, but the spatial precision remains low. However, STIMULUS outperforms TI and multielectrode TI stimulation in spatial precision, and also eliminates shallow stimulation observed in both these competing strategies.

Potential limitations due to idealized assumptions in our models, and how we could address them: We use idealized models, and the techniques need to be adapted to real head models. At least in part, we expect this process to be similar to adapting EEG spherical head model techniques to real heads, and results on beamforming in real-head models [20], [21] suggest that this should indeed be possible. This does require knowledge of conductances in different parts of the head, which can be aided by obtaining a structural MRI scan. However, limited knowledge of conductivity of different layers will limit the accuracy of our techniques. Techniques that advance on this understanding, e.g. electrical impedance tomography, improved imaging, and better estimation of tissue conductivity *in vivo*, can help with improved focusing.

While capacitive effects are not prominent at 250 Hz [27], tissues may have different dielectric properties under higher frequencies [36], and simulation studies have shown that electric field distribution induced by high frequency input (1000 Hz) can be significantly different from that induced by low-frequency inputs [37]. Future work will incorporate capacitive effects in the tissue. Such effects are equivalent to changing impedances and introducing frequency-dependent phase shifts. This amounts to a small change in our optimization problem by changing the forward matrix by incorporating induced phase changes in addition to amplitude changes.

The assumption of all neurons having the same orientation, while clearly incorrect, provides only a pessimistic estimation of attained spatial precision using our strategies because it disallows us from exploiting the diversity in orientation of different neurons to tailor currents. In practice, one can tailor currents to excite only neurons with desired orientation [38], which can be used to improve spatial precision of our stimulation.

Given the large freedom in configuring electrode-pair locations and waveforms, and concerns of tissue safety, in practice, one might need to further constrain the problem, e.g., by limiting currents from each electrode-pair, and further relax the problem by recognizing that approximate cancellation is still helpful.

Potential improvements on STIMULUS: We note that STIMULUS only provides a starting point to optimization approaches, and there are variations on the formulation that could improve precision. For example, instead of having foci for each patch-pair at the center of the target region, as is done here, one may want all electrode-patches to focus slightly off-center, creating “virtual sources” at these foci that are closer to each other than the electrodes. One may also want a different frequency allocation across electrodes for both STIMULUS and multielectrode TI stimulation.

While STIMULUS can largely reduce stimulation at undesired locations, as is shown in Section III, there are still voxels

(albeit very limited number) with such behavior. In order to fully address the issue, one may manually modify amplitudes of some of the electrode-pairs, use a different allocation of frequencies, or add further constraints to the optimization problem, e.g. spatial smoothness of activating functions.

Further, we need to understand tradeoffs between firing rate and spatial precision. For multielectrode TI stimulation, particularly when frequencies are allocated using our strategy, increasing spatial precision appears to be accompanied with reduced firing rate. However, the issue deserves a more thorough investigation. For example, it is plausible that an increase in base frequency can allow frequency differences to be larger as well.

Our results also suggest that TI stimulation may not work for certain types of neurons. This suggests that great care should be taken when applying TI to mammalian brains, where multiple neuron-types coexist. There is therefore a need to consider neuron-type selective stimulation. Finally, it may also be possible to use STIMULUS with implanted electrodes, and for stimulating the peripheral nervous system, as well as cochlear and retinal implants where localized stimulation is of immense importance.

REFERENCES

- [1] J. Cao and P. Grover, "Do single neuron models exhibit temporal interference stimulation?" in *IEEE Biomedical Circuits and Systems Conference (BioCAS)*, 2018, to appear. Available at <https://github.com/JiamingCao/Papers>.
- [2] T. Sato, M. G. Shapiro, and D. Y. Tsao, "Ultrasonic neuromodulation causes widespread cortical activation via an indirect auditory mechanism," *Neuron*, 2018.
- [3] H. Guo, M. Hamilton, S. J. Offutt, C. D. Gloeckner, T. Li, Y. Kim, W. Legon, J. K. Alford, and H. H. Lim, "Ultrasound produces extensive brain activation via a cochlear pathway," *Neuron*, 2018.
- [4] X. Niu, K. Yu, and B. He, "On the neuromodulatory pathways of the *in vivo* brain by means of transcranial focused ultrasound," *Current Opinion in Biomedical Engineering*, 2018.
- [5] N. Grossman, D. Bono, N. Dedic, S. B. Kodandaramaiyah, A. Rudenko, H.-J. Suk, A. M. Cassara, E. Neufeld, N. Kuster, L.-H. Tsai, A. Pascual-Leone, and E. S. Boyden, "Noninvasive deep brain stimulation via temporally interfering electric fields," *Cell*, vol. 169, no. 6, pp. 1029–1041, 2017.
- [6] R. H. Smith, "Electroanesthesia (ea), 1971," *Anesthesiology: The Journal of the American Society of Anesthesiologists*, vol. 34, no. 1, pp. 60–72, 1971.
- [7] G. Goats, "Interferential current therapy," *British journal of sports medicine*, vol. 24, no. 2, p. 87, 1990.
- [8] A. L. Hodgkin and A. F. Huxley, "A quantitative description of membrane current and its application to conduction and excitation in nerve," *The Journal of physiology*, vol. 117, no. 4, pp. 500–544, 1952.
- [9] Z. F. Mainen, J. Joerges, J. R. Huguenard, and T. J. Sejnowski, "A model of spike initiation in neocortical pyramidal neurons," *Neuron*, vol. 15, no. 6, pp. 1427–1439, 1995.
- [10] B. Chiovini, G. F. Turi, G. Katona, A. Kaszás, D. Pálfi, P. Maák, G. Szalay, M. F. Szabó, G. Szabó, Z. Szadai, S. Káli, and B. Rózsa, "Dendritic spikes induce ripples in parvalbumin interneurons during hippocampal sharp waves," *Neuron*, vol. 82, no. 4, pp. 908–924, May 2014.
- [11] B. Rózsa and S. Káli, personal communication.
- [12] B. Hutcheon and Y. Yarom, "Resonance, oscillation and the intrinsic frequency preferences of neurons," *Trends in neurosciences*, vol. 23, no. 5, pp. 216–222, 2000.
- [13] D. E. Goldman, "Potential, impedance, and rectification in membranes," *The Journal of general physiology*, vol. 27, no. 1, pp. 37–60, 1943.
- [14] B. Connors, M. Gutnick, and D. Prince, "Electrophysiological properties of neocortical neurons in vitro," *Journal of Neurophysiology*, vol. 48, no. 6, pp. 1302–1320, 1982.
- [15] P. L. Nunez and R. Srinivasan, *Electric Fields of the Brain: the Neurophysics of EEG*. Oxford University Press, 2006.
- [16] P. Grover and P. Venkatesh, "An information-theoretic view of EEG imaging," *Proceedings of the IEEE*, vol. 105, no. 2, pp. 367–384, Feb. 2017.
- [17] A. Datta, V. Bansal, J. Diaz, J. Patel, D. Reato, and M. Bikson, "Gyri-precise head model of transcranial direct current stimulation: improved spatial focality using a ring electrode versus conventional rectangular pad," *Brain stimulation*, vol. 2, no. 4, pp. 201–207, 2009.
- [18] A. Datta, M. Elwassif, F. Battaglia, and M. Bikson, "Transcranial current stimulation focality using disc and ring electrode configurations: FEM analysis," *Journal of neural engineering*, vol. 5, no. 2, p. 163, 2008.
- [19] H. Seo and S. C. Jun, "Relation between the electric field and activation of cortical neurons in transcranial electrical stimulation," *Brain stimulation*, 2018.
- [20] G. Ruffini, M. D. Fox, O. Ripolles, P. C. Miranda, and A. Pascual-Leone, "Optimization of multifocal transcranial current stimulation for weighted cortical pattern targeting from realistic modeling of electric fields," *Neuroimage*, vol. 89, pp. 216–225, 2014.
- [21] J. P. Dmochowski, A. Datta, M. Bikson, Y. Su, and L. C. Parra, "Optimized multi-electrode stimulation increases focality and intensity at target," *Journal of neural engineering*, vol. 8, no. 4, p. 046011, 2011.
- [22] R. Kempe, Y. Huang, and L. C. Parra, "Simulating pad-electrodes with high-definition arrays in transcranial electric stimulation," *Journal of neural engineering*, vol. 11, no. 2, p. 026003, 2014.
- [23] M. Mahmud and S. Vassanelli, "Differential modulation of excitatory and inhibitory neurons during periodic stimulation," *Frontiers in neuroscience*, vol. 10, p. 62, 2016.
- [24] B. D. Van Veen and K. M. Buckley, "Beamforming: A versatile approach to spatial filtering," *IEEE Acoustics, Speech, and Signal Processing (ASSP) magazine*, vol. 5, no. 2, pp. 4–24, 1988.
- [25] J. M. Godlove, E. O. Whaite, and A. P. Batista, "Comparing temporal aspects of visual, tactile, and microstimulation feedback for motor control," *Journal of neural engineering*, vol. 11, no. 4, 2014.
- [26] J. E. O'Doherty, M. A. Lebedev, P. J. Ifft, K. Z. Zhuang, S. Shokur, H. Bleuler, and M. A. Nicolelis, "Active tactile exploration using a brain-machine-brain interface," *Nature*, vol. 479, no. 7372, pp. 228–231, 2011.
- [27] A. Opitz, A. Falchier, C.-G. Yan, E. M. Yeagle, G. S. Linn, P. Megevand, A. Thielscher, M. P. Milham, A. D. Mehta, and C. E. Schroeder, "Spatiotemporal structure of intracranial electric fields induced by transcranial electric stimulation in humans and nonhuman primates," *Nature Scientific reports*, vol. 6, p. 31236, 2016.
- [28] J. Vorwerk, R. Oostenveld, M. C. Piastra, L. Magyari, and C. H. Wolters, "The FieldTrip-SimBio pipeline for EEG forward solutions," *Biomedical engineering online*, vol. 17, no. 1, p. 37, 2018.
- [29] F. Rattay, "Analysis of models for external stimulation of axons," *IEEE transactions on biomedical engineering*, no. 10, pp. 974–977, 1986.
- [30] E. M. Izhikevich, *Dynamical systems in neuroscience*. MIT press, 2007.
- [31] P. J. Basser and B. J. Roth, "New currents in electrical stimulation of excitable tissues," *Annual review of biomedical engineering*, vol. 2, no. 1, pp. 377–397, 2000.
- [32] S. Joucla and B. Yvert, "Modeling extracellular electrical neural stimulation: from basic understanding to MEA-based applications," *Journal of Physiology-Paris*, vol. 106, no. 3-4, pp. 146–158, 2012.
- [33] J. R. Dormand and P. J. Prince, "A family of embedded Runge-Kutta formulae," *Journal of computational and applied mathematics*, vol. 6, no. 1, pp. 19–26, 1980.
- [34] Y. Zhang, W. van Drongelen, and B. He, "Estimation of *in vivo* brain-to-skull conductivity ratio in humans," *Applied physics letters*, vol. 89, no. 22, 2006.
- [35] A. V. Oppenheim, A. S. Willsky, and S. H. Nawab, *Signals and Systems (2Nd Ed.)*. Upper Saddle River, NJ, USA: Prentice-Hall, Inc., 1996.
- [36] S. Gabriel, R. Lau, and C. Gabriel, "The dielectric properties of biological tissues: III. parametric models for the dielectric spectrum of tissues," *Physics in medicine and biology*, vol. 41, no. 11, p. 2271, 1996.
- [37] Z. Manoli, N. Grossman, and T. Samaras, "Theoretical investigation of transcranial alternating current stimulation using realistic head model," in *IEEE Engineering in Medicine and Biology Conference (EMBC)*, 2012, pp. 4156–4159.
- [38] C. Terzuolo and T. Bullock, "Measurement of imposed voltage gradient adequate to modulate neuronal firing," *Proceedings of the National Academy of Sciences*, vol. 42, no. 9, pp. 687–694, 1956.

APPENDIX

As we discussed, there is significant variation in estimates of skull conductivity in the literature (e.g., [34], [15]). In this

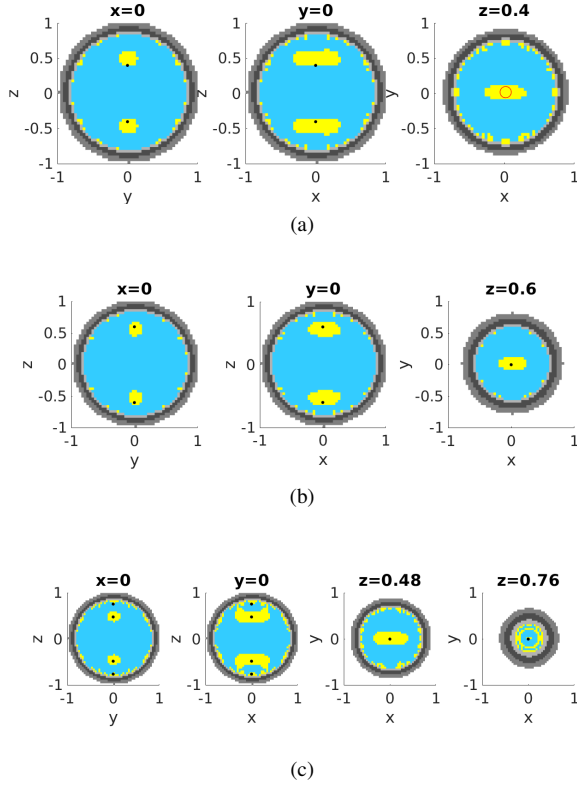


Fig. 12. STIMULUS when assuming $\sigma_1/\sigma_3 = 1/80$, classical HH neuron is used. (a) Focusing at [0,0,0.4] (b) Steerable stimulation; focusing at [0,0,0.6] (c) Multisite stimulation; focusing at [0,0,0.52] and [0,0,0.76] simultaneously. Yellow: stimulation; Gray layers from outside to inside: scalp, skull, and CSF. Focus points are indicated by black dots, and target regions are indicated by red circles.

section, we observe the performance of STIMULUS when assuming a lower conductivity of skull, where $\sigma_1/\sigma_3 = 1/80$ [15]. For illustration, only the classical HH neuron is used here. Target regions, frequency allocations, as well as geometrical arrangement of electrode-pairs are chosen to be the same as in Table II. Results are shown in Fig. 12. It can be observed that the performance is qualitatively similar to those shown in Fig. 8c, Fig. 10 and Fig. 11, where $\sigma_1/\sigma_3 = 1/15$ is assumed.